Fermi National Accelerator Laboratory

FERMILAB-Conf-83/13-EXP
7550.537

A COMPARISON OF DIMUON PRODUCTION BY 125 GeV/c $\bar{p}$ AND π^- WITH PREDICTIONS OF THE DRELL-YAN MODEL*

B. Cox

January 1983

*Invited talk presented at the Drell-Yan Workshop, Fermilab, October 1982

FERMILAB-Conf-83/13-EXP

A COMPARISON OF DIMUON PRODUCTION BY 125 GeV/c $\bar{p}$ and π^- WITH PREDICTIONS OF THE DRELL-YAN MODEL

B. Cox
Fermi National Accelerator Laboratory
P.O. Box, Batavia, Illinois 60510

Abstract

The measurements of dimuon production ($M > 4$ GeV/c^2) by 125 GeV/c $\bar{p}$ and π^- performed by Fermilab Experiment 537 are compared to the predictions of the Drell-Yan model in this report. We find that the naive Drell-Yan cross sections calculated using CDHS and NA3 structure functions are too low by factors of 2.25 ± 0.45 and 2.50 ± 0.50 to reproduce the levels of our $\bar{p}$ and π^- cross sections respectively. The shapes of the $d\sigma/dx_F$ and $M^3\, d\sigma/dM$ differential cross sections are well reproduced by the naive zeroth order formula. The shape of the $d\sigma/dp_T$ cross section for the dimuons as measured by E-537 can be fit using the Altarelli, Parisi, and Petronzio $O(\alpha_s)$ prescription for calculating p_T distributions but requires a $\langle k_T^2 \rangle$ of the interacting constituents of the nucleons and pion of 0.88 $(GeV/c)^2$. This $\langle k_T^2 \rangle$ is larger than the $\langle k_T^2 \rangle_\pi = 0.59 \pm 0.05$ $(GeV/c)^2$ and $\langle k_T^2 \rangle_p = 0.52 \pm 0.05$ $(GeV/c)^2$ obtained from the linear extrapolations of the s variation of the $\langle p_T^2 \rangle$ of the experimentally observed $d\sigma/dp_T$ distributions to s=0. This implies that first order QCD in the formalism of Altarelli, Parisi, and Petronzio is insufficient to explain $\langle p_T^2 \rangle$ of the data.

High mass dimuon production in hadronic interactions has been interpreted as proceeding via the Drell-Yan[1] process and higher order QCD processes[2] (Fig. 1). Measurements of hadronic production of dimuons and especially the measurement of $\bar{p}$ production of dimuons test the QCD picture of these reactions as proceeding via the strong interactions of the constituents of the hadrons. In the particular case of $\bar{p}N \to \mu^+\mu^- + X$ the valence quark structure functions of the nucleons can be determined independently from deep inelastic lepton scattering experiments, thereby allowing a more complete confrontation of the theory than is possible in either π or K production of dimuons.

A Fermilab-Athens-McGill-Michigan collaboration has studied the production of dimuons by $\bar{p}$ and π^- at 125 GeV/c using a special enriched antiproton beam derived from $\bar{\Lambda}^o \to \bar{p}\pi$ decay (Fig. 2). This experiment was performed in the High Intensity Laboratory at Fermilab. We were able to routinely obtain from this beam 10^7 125 GeV/c particles per second of spill with 5 x 10^{12} 400 GeV protons incident on the secondary beam production target. This 10^7 secondary beam had a composition of 20% antiprotons and 80% π^- (from $K^o_s \to \pi^-\pi^+$ decays). The momentum, direction and identity of this large momentum bite ($\Delta p/p \backsim \pm 10\%$) beam were measured and tagged on an event by event basis. In less than 800 hours of data taking using the large aperture forward spectrometer shown in Fig. 3, the dimuon mass spectra shown in Fig. 4a and 4b were accumulated. The mass resolution ($\sigma \backsim 190$ MeV/c^2) of the $\psi(3.1)$ was dominated by the error in the dimuon opening angle caused by multiple scattering in the heavy nuclear targets (Cu, W) and in the 60" copper hadron absorber. The error introduced by momentum measurement inaccuracy was minimized by the precision of the E-537 drift chamber system ($\sigma_x \backsim 250\mu$) and the strength of the analysis magnet ($\Delta p_T \backsim 0.8$ GeV/c). The spectrometer and

the beam have been described elsewhere[3,4,5] and will not be discussed further here.

We have used the standard Drell-Yan formula (Fig. 1a)

$$\frac{d\sigma}{dMdx_F} = \frac{8\pi\alpha^2}{9M^3}\frac{\tau}{\sqrt{x_F^2 + 4\tau}}\sum_i e_i^2\left[q_i^{h_1}(x_1)\,\bar{q}_2^{h_2}(x_2) + (1 \leftrightarrow 2)\right] \qquad (1)$$

where $\tau = M^2/s = x_1 x_2$ and $x_F = x_1 - x_2$ to calculate the differential cross sections $M^3\ d\sigma/dM$ and $d\sigma/dx_F$ for dimuons production by 125 GeV/c $\bar{p}$ and π^-. We have used the CDHS structure functions[6] for the nucleon and antinucleon and the NA3 structure functions[7] for the π^-. These structure functions are given below in Table I:

Table I

Hadronic Structure Functions Used in the Drell-Yan Calculations Contained in this Report

$xu_p = u_o x^{0.52-0.16\bar{s}}\,(1-x)^{2.79+0.77\bar{s}}$	CDHS (Ref. 6)
$xd_p = d_o x^{0.52-0.16\bar{s}}\,(1-x)^{3.79+0.77\bar{s}}$	CDHS (Ref. 6)
$xs_p = (0.26+0.18\bar{s})\,(1-x)^{7.80+0.78\bar{s}}$	CDHS (Ref. 6)
$xG_p = 3.06(1-x)^{5.0}$	Counting rules
$xV_\pi = V_o x^{0.4}(1-x)^{0.9}$	NA3 (Ref. 7)
$xS_\pi = 0.24(1-x)^{6.9}$	NA3 (Ref. 7)
$xG_\pi = 2(1-x)^{3.0}$	Counting rules

In Table I the $Q^2 = M^2$ evolution variable is $\bar{s} = \ell n\left[\ell n(M^2/\Lambda^2)/\ell n(20/\Lambda^2)\right]$ where Λ is taken to be 0.5. Figure 5 shows the $d\sigma/dx_F$ differential cross section obtained by E-537 for the $\bar{p}$ and π^- along with the Drell-Yan predictions from

(1). The Drell-Yan prediction has been multiplied by a K factor = 2.25 ± 0.45 for the $\bar{p}$ data and by 2.50 ± 0.50 for the π^- data. The shape of the x_F distribution is quite well fit by the Drell-Yan calculation. Figure 6 shows M^3 $d\sigma/dM$ from E-537 and NA3 for the antiproton reaction. Once again the prediction of Eq. (1) for M^3 $d\sigma/dM$ matches quite well the shape of the dimuon differential cross section but the level of the Drell-Yan prediction has to be multiplied by 2.25 to match the level of the data.

Going beyond the simple Drell-Yan formula (1), we have attempted to calculate the differential cross section $1/p_T$ $d\sigma/dp_T$ that we should observe in our data using the $O(\alpha_s)$ formula[2] for dimuon production by the Compton (σ_C) and annihilation (σ_A) processes (Figs. 1b and 1c) given below:

$$\frac{d\sigma_P}{dM\ dy\ dp_T^2} = \frac{d\sigma_A}{dM\ dy\ dp_T^2} + \frac{d\sigma_C}{dM\ dy\ dp_T^2}$$

$$= \frac{16\alpha^2}{27}\ \frac{s}{M}\int_{x_1^{min}}^{1} dx_1\ \frac{x_1x_2\alpha_s}{x_1s+u-M^2}\ \frac{(\hat{t}-M^2)^2+(\hat{u}-M^2)^2}{s^2\hat{t}\hat{u}}\cdot\sum_i e_i^2\left[q_i^{h_1}(x_1,Q^2)\,\bar{q}_i^{h_2}(x_2,Q^2)+(1\leftrightarrow 2)\right]$$

$$+\ \frac{2\alpha^2}{9}\ \frac{s}{M}\int_{x_1^{min}}^{1} dx_1\ \frac{x_1x_2\alpha_s}{x_1s+u-M^2}\ \frac{\hat{s}^2+\hat{u}^2+2M^2\hat{t}}{-\hat{s}^3\hat{u}}\cdot\sum_i e_i^2\left[q_i^{h_1}(x_1,Q^2)\,G_i^{h_2}(x_2,Q^2)+(1\leftrightarrow 2)\right] \qquad (2)$$

We have used (2) in the Altarelli, Parisi, and Petronzio[8] prescription

$$\frac{d\sigma}{dM\ dy\ dp_T^2} = \pi f(p_T)\frac{d\sigma_{DY}}{dM\ dy} + \int d^2q_T \frac{d\sigma_P}{dM\ dy\ dp_T^2}\ [f(\vec{p}_T-\vec{q}_T)-f(p_T)] \qquad (3)$$

in order to incorporate the intrinsic k_T of the interacting constituents. $f(p_T)$ is assumed to be a Gaussian distribution with the normalization

$$\int f(p_T) d^2p_T = \frac{1}{\pi \langle k_T^2 \rangle} \int d^2p_T \exp[-p_T^2/\langle k_T^2 \rangle] = 1 \qquad (4)$$

Figure 7 shows $1/p_T \; d\sigma/dp_T$ for the E-537 $\bar{p}$ and π^- data along with the predictions obtained from using (2), (3) and (4). In order to fit the $\bar{p}$ and π^- data, $d\sigma/(dM\, dy\, dp_T^2)$ has been multiplied by the K factors mentioned above. These K factors have been assumed to be independent of τ, x_F and p_T and $\langle k_T^2 \rangle$ has been given the value 0.88 GeV/c^2. The contributions of the various components, σ_A, σ_C and the Gaussian describing the intrinsic k_T are shown in Fig. 7. As can be expected, the QCD diagrams (Fig. 1b and 1c) begin to contribute beyond p_T = 2 GeV/c with the annihilation diagram contributing more than the Compton diagram because of the presence of the valence antiquarks in both the $\bar{p}$ and π^-.

The technique outlined above requires that $\langle k_T^2 \rangle$ = 0.88 GeV/c for the interacting constituents in order to achieve reasonable fits to the p_T distribution. As pointed out in Ref. 9, the $\langle k_T^2 \rangle$ of the constituents can be determined by examining the s dependence of the second momenta $\langle p_T^2 \rangle$ of the p_T distributions for the existing data for p, $\bar{p}$, and π^- production of dimuons. Figure 8a and b show that the $\langle p_T^2 \rangle$ data for dimuon production varies nearly linearly with s for protons and π^-. The data from E-537 and NA3 for antiprotons shown in Fig. 8a is not as precise as that for p and π^-. The $\bar{p}$ data does however appear to have $\langle p_T^2 \rangle$ similar to the π^- induced dimuons but slightly lower at the three values of s at which there are measurements. The extrapolation of a linear fit of this data ($\langle p_T^2 \rangle$ = A+Bs) to s=0 should yield $\langle k_T^2 \rangle$ of the interacting constituents. As shown in Fig. 8, these intercepts are 0.59 ± 0.05 $(GeV/c)^2$ and 0.52 ± 0.05 $(GeV/c)^2$ for the π^- and p data respectively. The difference between these values and the larger value of

$\langle k_T^2 \rangle = 0.88$ GeV/c^2 required to fit the E-537 125 GeV/c $\bar{p}$ and π^- data suggests that the $O(\alpha_s)$ prescription of Altarelli et al., is insufficient to explain the $\langle p_T^2 \rangle$ of dimuon data. Indeed as pointed out in Ref. 9 when (2), (3) and (4) with $\langle k_T^2 \rangle_{\pi^-} = 0.59$ $(GeV/c)^2$ and $\langle k_T^2 \rangle_p = 0.52$ $(GeV/c)^2$ are used to calculate $\langle p_T^2 \rangle$ as a function of s, the values of $\langle p_T^2 \rangle$ obtained are consistently below the existing data at all energies.

In conclusion, we find that the simple Drell-Yan formalism is sufficient to predict the shapes of the M^3 $d\sigma/dM$ and the $d\sigma/dx_F$ distributions of the E-537 $\bar{p}$ and π^- data but is unable to predict the level of the cross sections. Attempts to fit the shape of the p_T distributions require including $O(\alpha_s)$ QCD effects to make the high p_T tail of the observed distributions. The Altarelli, Parisi and Petronzio prescription for calculating $1/p_T$ $d\sigma/dp_T$ requires an intrinsic $\langle k_T^2 \rangle = 0.88$ GeV/c^2 which is larger than those ($\langle k_T^2 \rangle_\pi = 0.59 \pm 0.05$ GeV/c^2, $\langle k_T^2 \rangle_p = 0.52 \pm 0.05$ GeV/c^2) obtained by the extrapolation of observed linear behavior of $\langle p_T^2 \rangle$ vs. s to s=0. This implies that higher order QCD effects must be taken into account in order to explain the p_T distributions of dimuons.

The individuals who have collaborated to produce the E-537 measurements shown in this paper are M. Binkley, B. Cox, J. Enagonio, C. Hojvat, D. Judd, R. D. Kephart, P. K. Malhotra, P. O. Mazur, C. T. Murphy, F. Turkot, R. L. Wagner, D. Wagoner, and W. Yang -- Fermilab; E. Anassontzis, S. Katsavevas, P. Kostarakis, C. Kourkoukalis, A. Markou, L. K. Resvanis, G. Voulgaris -- University of Athens; H. Areti, S. Conetti, P. LeBrun, D. Ryan, T. Ryan, W. Schappert, D. Stairs -- McGill University; C. Akerlof, P. Kraushaar, D. Nitz, R. Thun -- University of Michigan; and He Mao, Zhang Nai-jian -- Shandong University. We wish to thank Fermilab, The U. S. Department of Energy, the National Science Foundation International Programs and High Energy Physics Divisions, the Natural Sciences and Engineering Research Council of Canada, Quebec Department of Education, and the Hellenic Science and Technology Agency for their support.

References

1. S.D. Drell and T.-M. Yan, Phys. Rev. Lett. 25, 316 (1970).

2. F. Halzen and D.M. Scott, Phys. Rev. D18, 3378 (1978).

3. B. Cox, Fermilab Report 79/1, 0090.01, January (1979).

4. Anassontzis, E., et al., Paper 665, XXI International Conference on High Energy Physics, Paris, France, 1982/Fermilab Preprint, Conf-82/50-EXP.

5. Anassontzis, E. et al., Paper 656, XXI International Conference on High Energy Physics, Paris, France, 1982/Fermilab Preprint, Conf-82/49-EXP.

6. J.G.H. deGroot et al., CDHS Collaboration, Phys. Lett. 82B, 455 (1979).

7. D. DeCamp, NA3 Collaboration, Proceedings of the XX International Conference on High Energy Physics, Madison, 149 (1980).

8. G. Altarelli et al., Phys. Lett. 76B, 356 (1978).

9. B. Cox and P.K. Malhotra, Fermilab-Pub-82/99-Exp.

Figure Captions

Fig. 1. (a) Naive Drell-Yan process.

(b) $O(\alpha_s)$ quark-antiquark annihilation process.

(c) $O(\alpha_s)$ gluon-quark Compton scattering.

Fig. 2. Schematic of the enriched antiproton beam obtained from $\bar{\Lambda} \to \bar{p}\pi^+$ decay used in E-537.

Fig. 3. E-537 spectrometer.

Fig. 4. (a) Mass spectrum of dimuons obtained in 125 GeV/c π^-N interactions measured by E-537.

(b) Mass spectrum of dimuons obtained in 125 GeV/c $\bar{p}$N interactions measured by E-537.

Fig. 5. Differential cross sections $d\sigma/dx_F$ for $M > 4$ GeV/c^2 dimuon events from antiproton and π^- reactions at 125 GeV/c. The curves are the predictions obtained using the simple Drell-Yan formula, the CDHS and NA3 structure functions, and the renormalizing K factors given in the text.

Fig. 6. The scaling cross section $M^3\, d\sigma/dM$ ($x_F > 0$) for 125 GeV/c $\bar{p}$ induced dimuons. The curve is the prediction of the Drell-Yan model using CDHS structure functions and a K factor of 2.25.

Fig. 7. The $1/p_T\, d\sigma/dp_T$ differential cross sections of $\bar{p}$ and π^- induced dimuons as measured by E-537. The solid curves are the predictions for these distributions obtained using the $O(\alpha_s)$ Altarelli, Parini and Petronzio prescription and a $\langle k_T^2 \rangle$ of the interacting constituents of 0.88 (GeV/c)^2. The various contributions (Compton, annihilation and intrinsic) to the p_T are shown by the dotted and dashed curves.

Fig. 8. (a) $\langle p_T^2 \rangle$ vs. s for π^- and $\bar{p}$ induced dimuons.

(b) $\langle p_T^2 \rangle$ vs. s for proton induced dimuons.

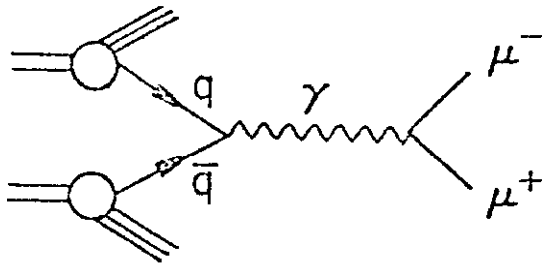

(a)

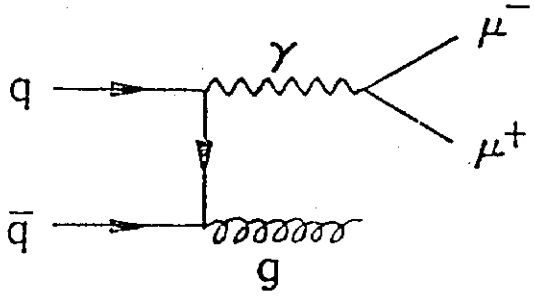

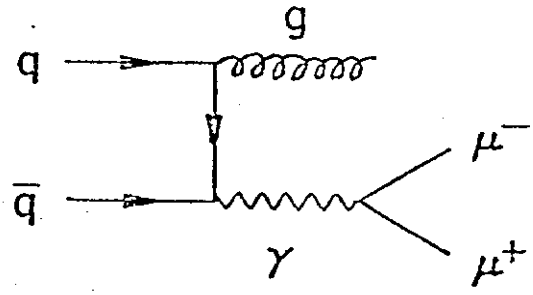

(b)

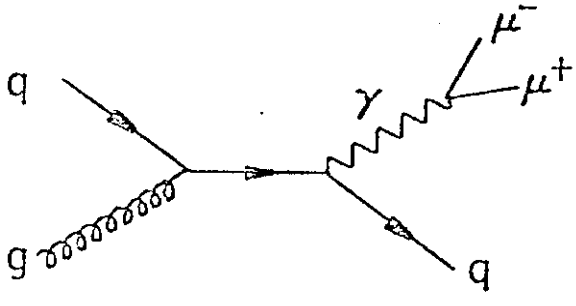

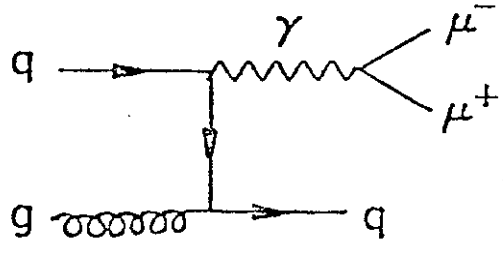

(c)

Fig. 1

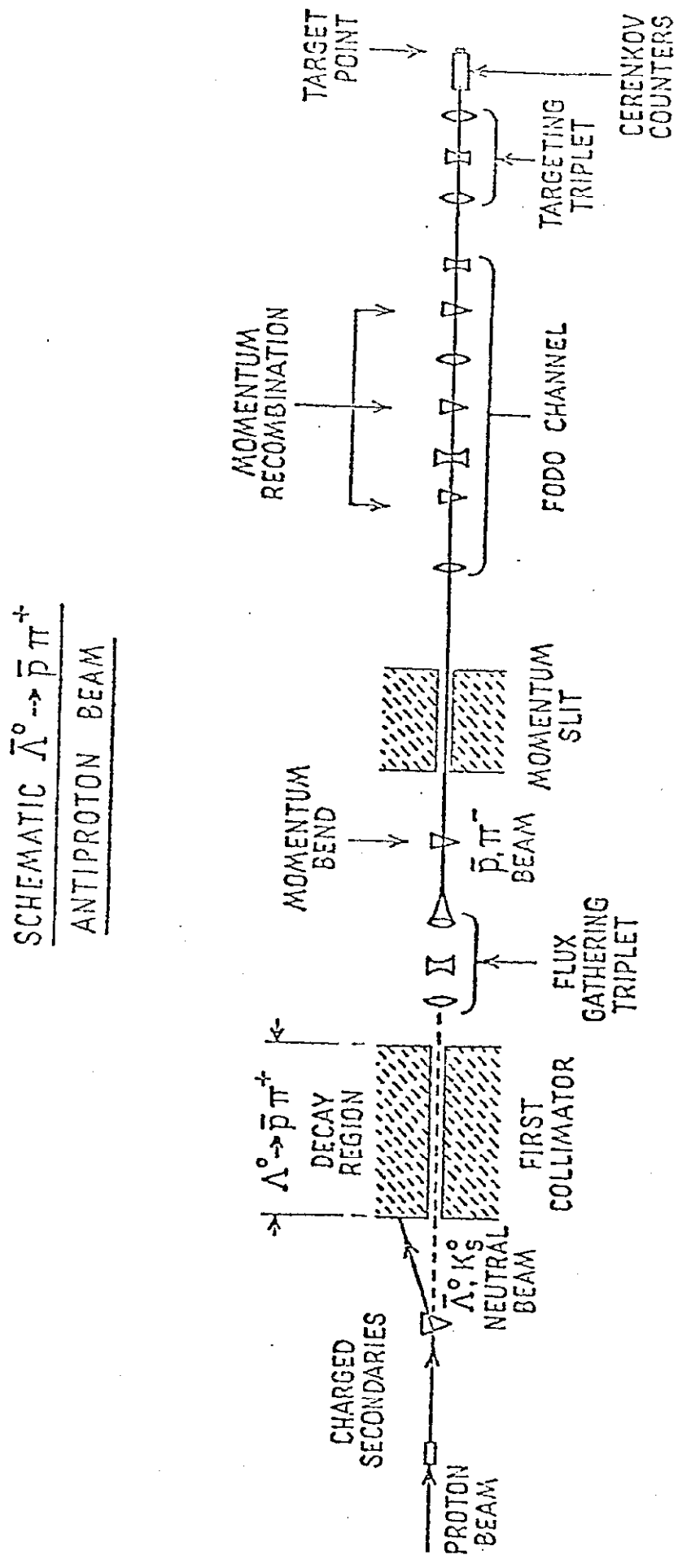
SCHEMATIC $\bar{\Lambda}^0 \to \bar{p}\pi^+$
ANTIPROTON BEAM
PROTON BEAM
CHARGED SECONDARIES
$\bar{\Lambda}^0, K^0_S$ NEUTRAL BEAM
$\Lambda^0 \to \bar{p}\pi^+$ DECAY REGION
FIRST COLLIMATOR
FLUX GATHERING TRIPLET
MOMENTUM BEND
$\bar{p}, \pi^-$ BEAM
MOMENTUM SLIT
MOMENTUM RECOMBINATION
FODO CHANNEL
TARGETING TRIPLET
TARGET POINT
CERENKOV COUNTERS

Fig. 2

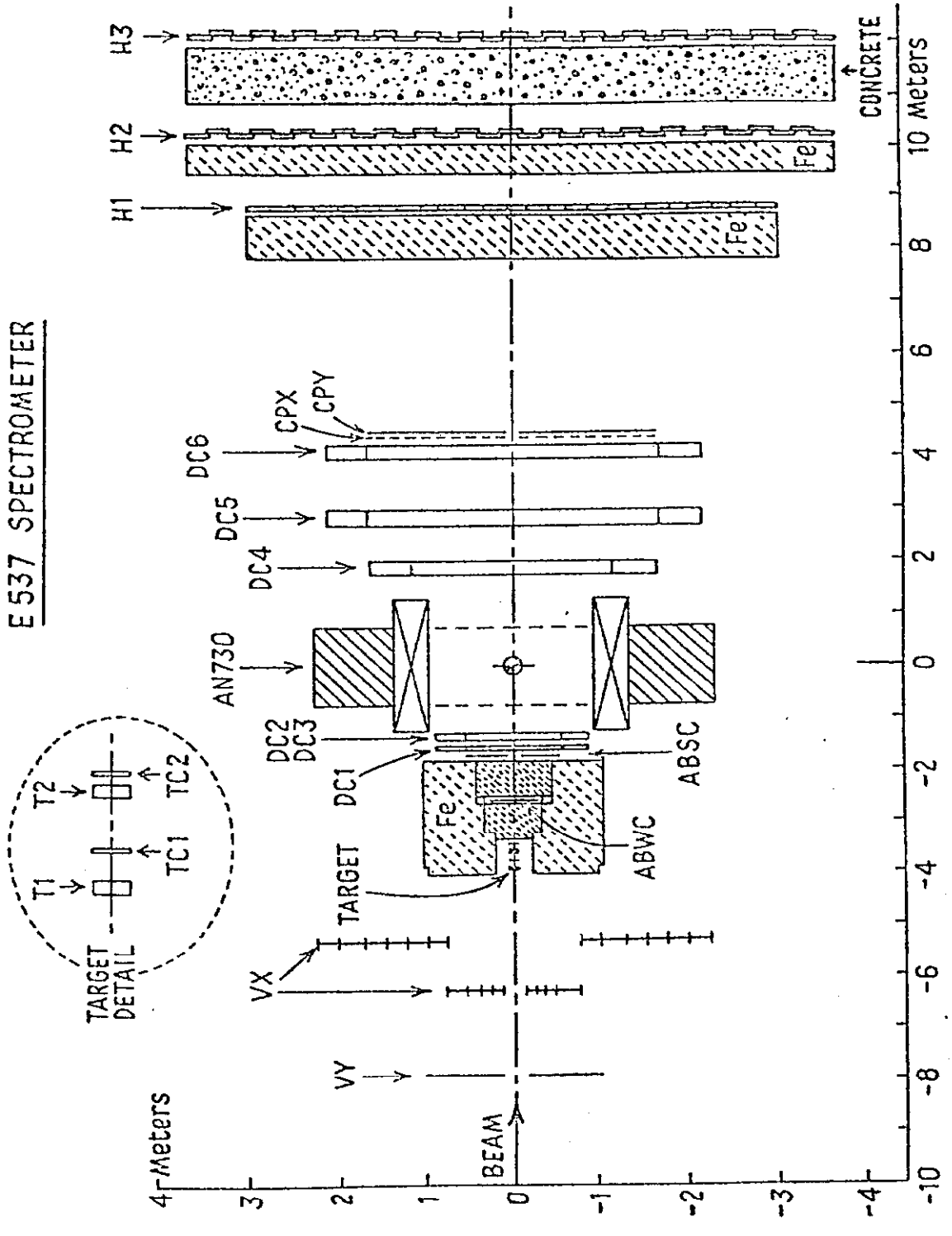
E537 SPECTROMETER
H3
H2
H1
Fe
Fe
CONCRETE
10 Meters
CPX
CPY
DC6
DC5
DC4
AN730
DC2
DC3
DC1
Fe
ABSC
ABWC
TARGET
VX
VY
BEAM
4 Meters
TARGET DETAIL
T1
T2
TC1
TC2

Fig. 3

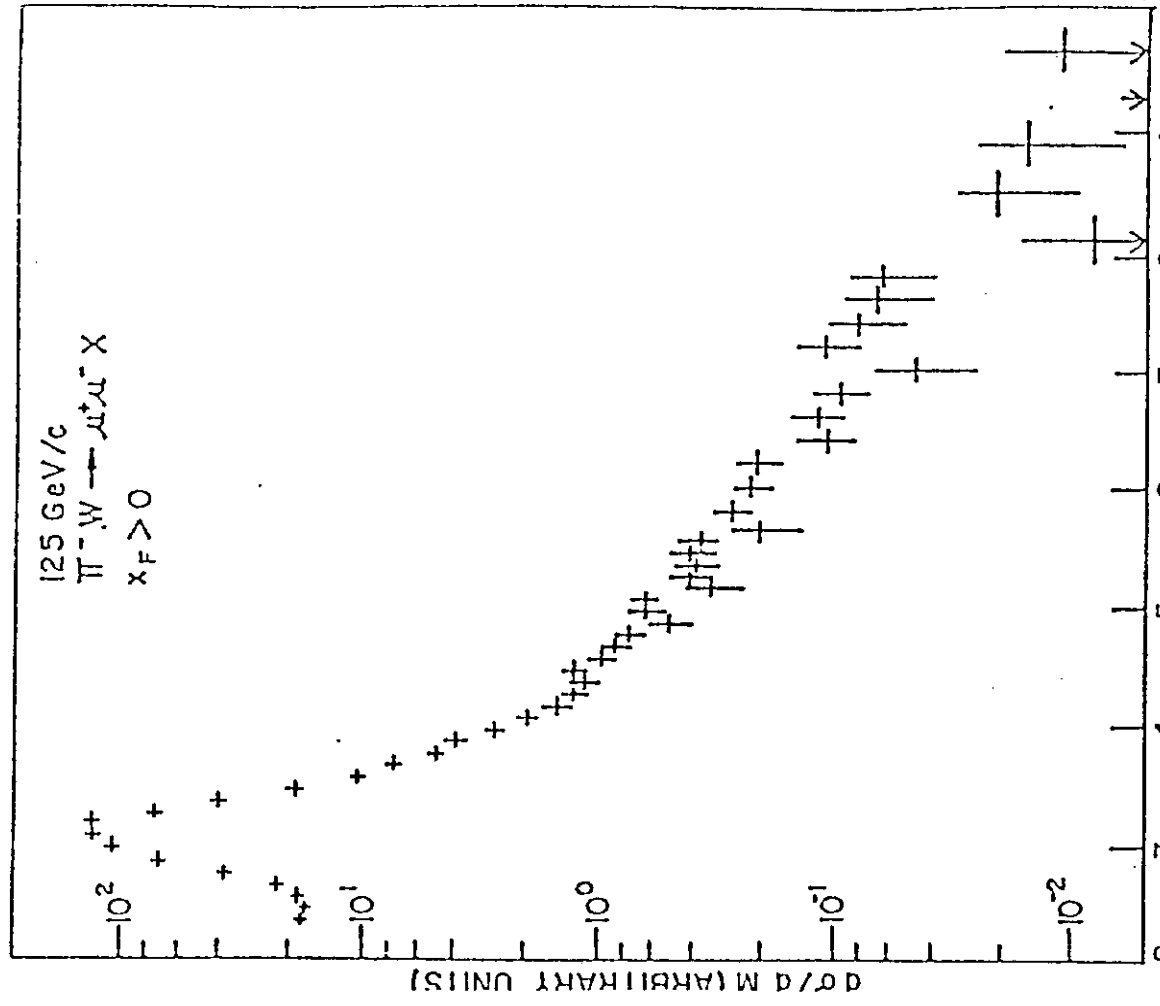
125 GeV/c
$\pi^- W \rightarrow \mu^+\mu^- X$
$x_F > 0$
$d\sigma/dM$ (ARBITRARY UNITS)
M (GeV/c²)

Fig. 4b

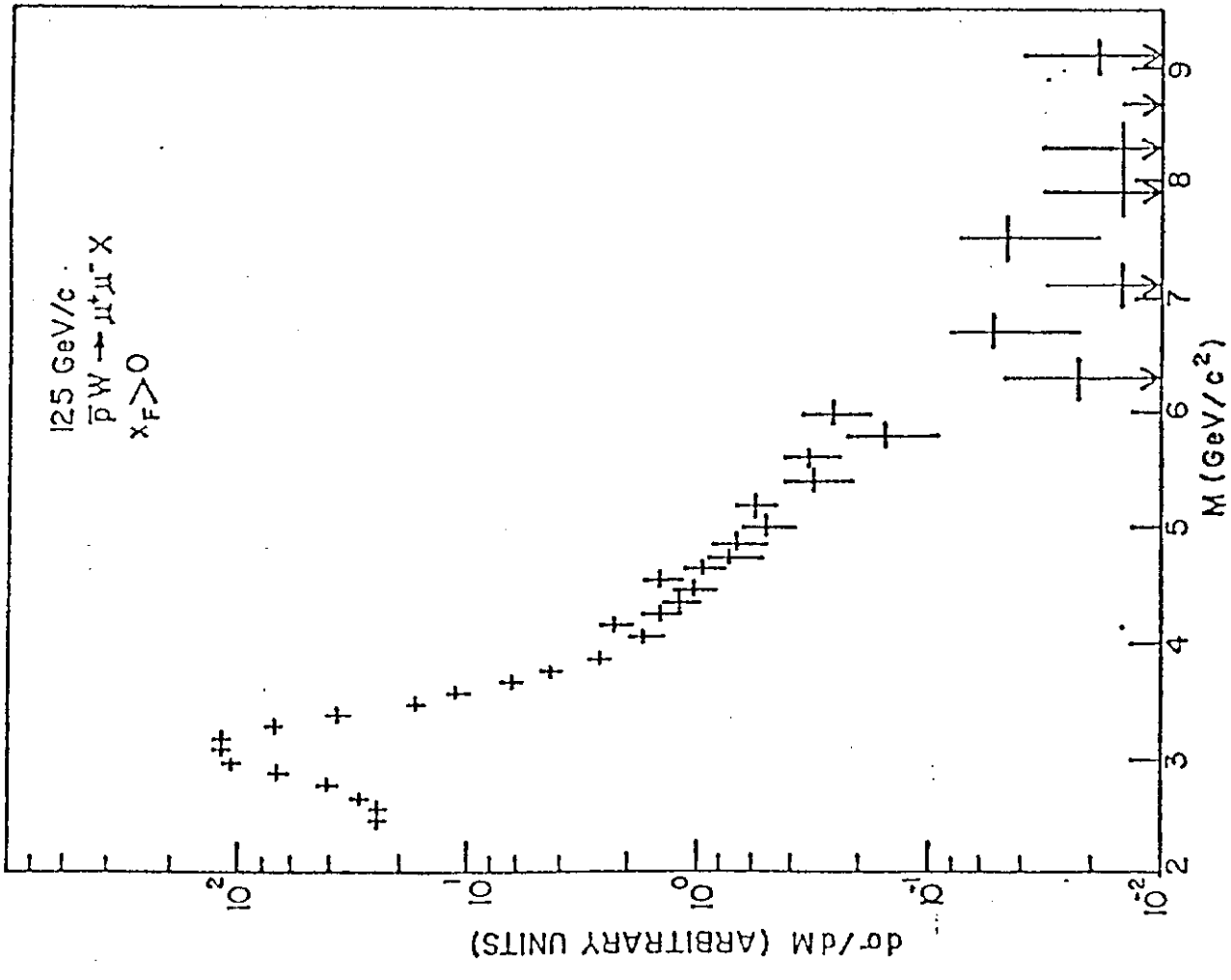
125 GeV/c
$\bar{p} W \rightarrow \mu^+\mu^- X$
$x_F > 0$
$d\sigma/dM$ (ARBITRARY UNITS)
M (GeV/c²)

Fig. 4a

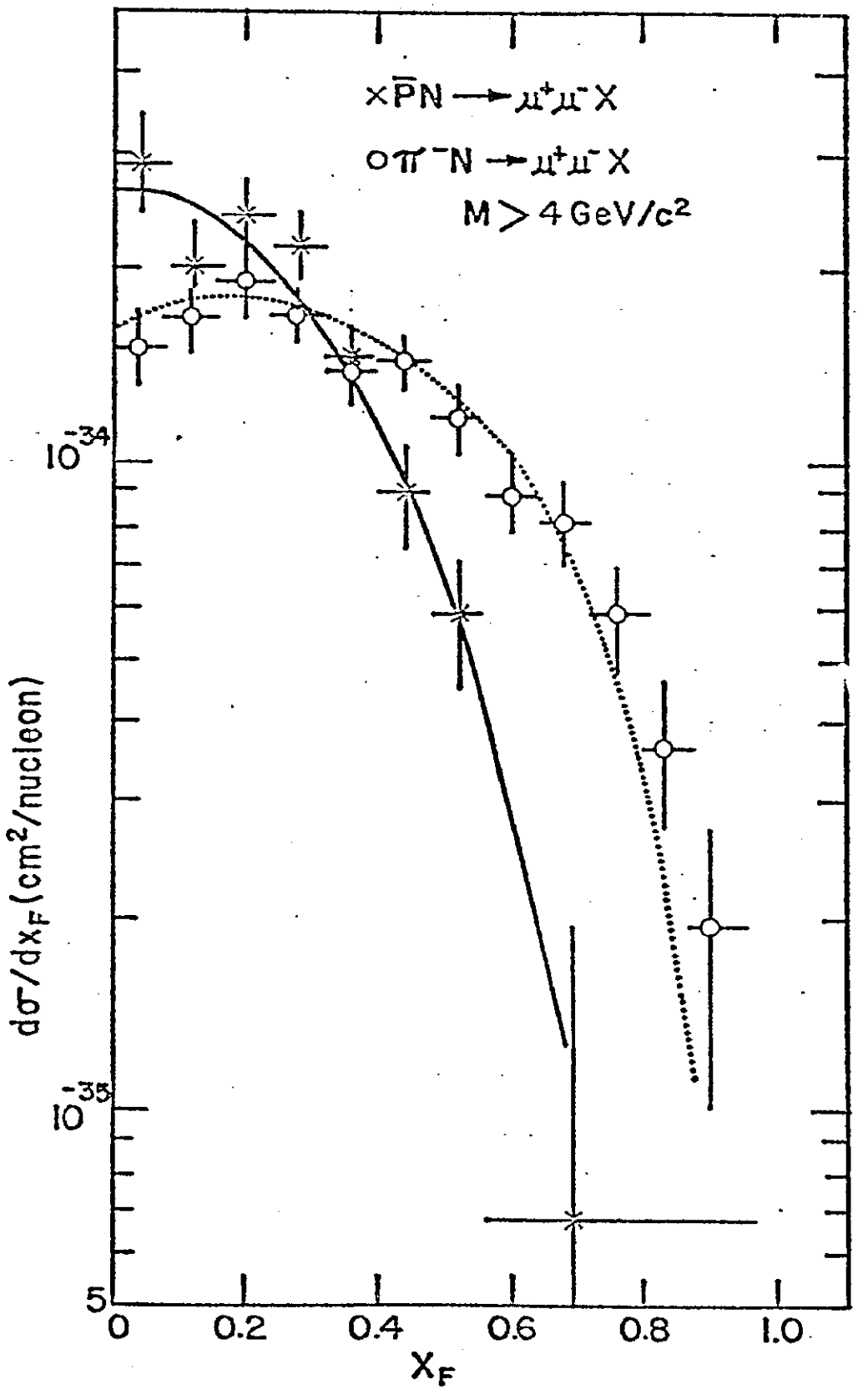
×P̄N → μ⁺μ⁻X
○π⁻N → μ⁺μ⁻X
M > 4 GeV/c²
10⁻³⁴
10⁻³⁵
5
dσ/dx_F (cm²/nucleon)
0
0.2
0.4
0.6
0.8
1.0
X_F

Fig. 5

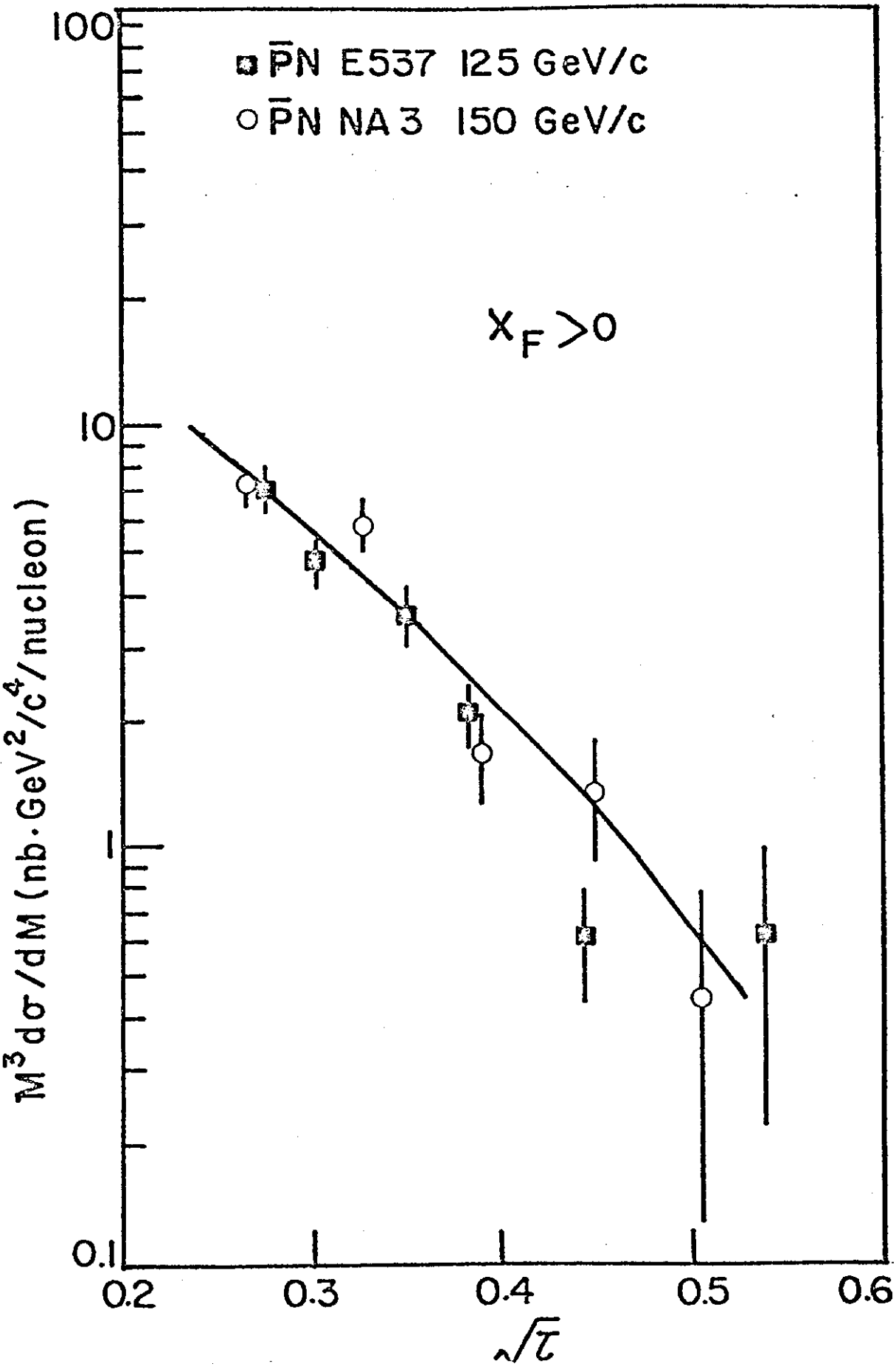
100
10
1
0.1
0.2
0.3
0.4
0.5
0.6
$\sqrt{\tau}$
$M^3 d\sigma/dM$ (nb·GeV^2/c^4/nucleon)
$\bar{P}N$ E537 125 GeV/c
$\bar{P}N$ NA 3 150 GeV/c
$X_F > 0$

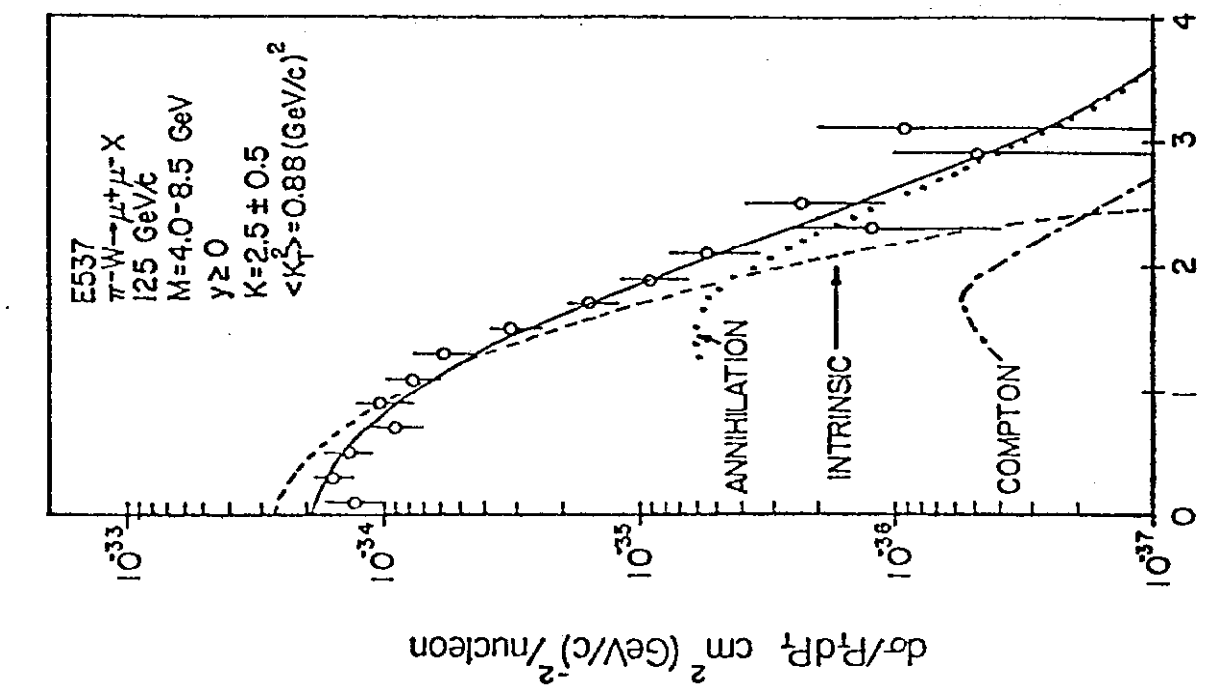
E537
$\pi^- W \to \mu^+\mu^- X$
125 GeV/c
M=4.0-8.5 GeV
y≥0
K=2.5 ± 0.5
$\langle K_T^2 \rangle = 0.88$ (GeV/c)^2
ANNIHILATION
INTRINSIC
COMPTON
$d\sigma/P_T dP_T$ cm^2 (GeV/c)$^{-2}$/nucleon
P_T (GeV/c)

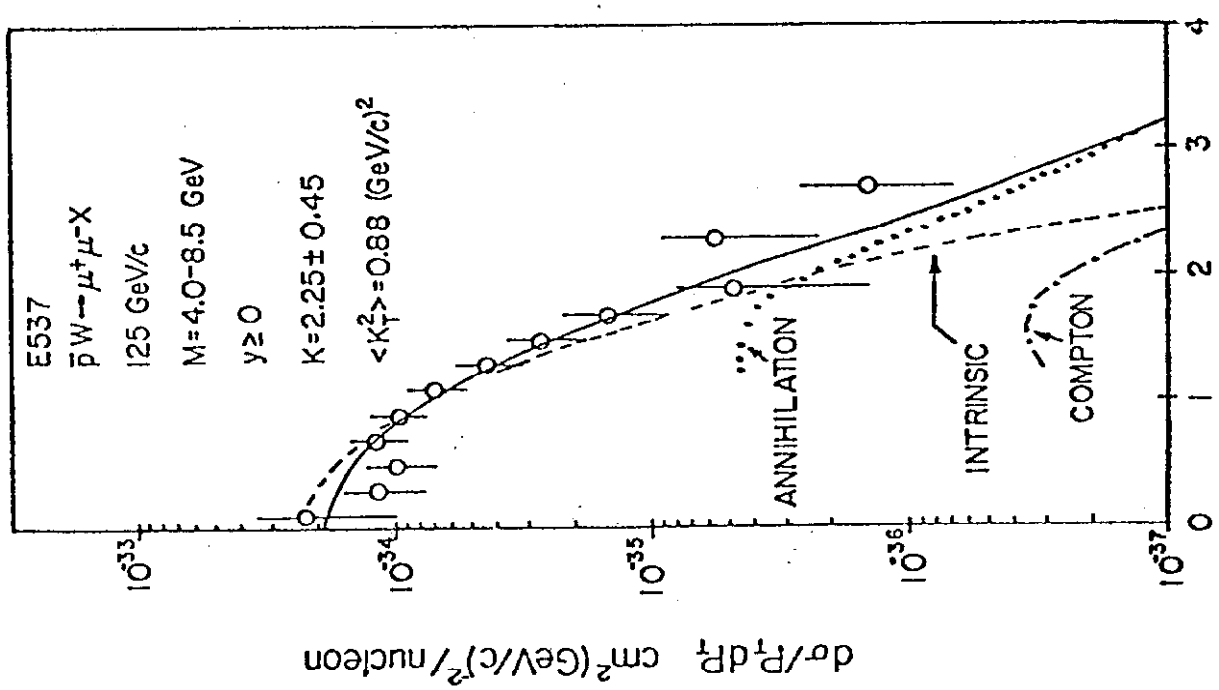
E537
$\bar{p} W \to \mu^+\mu^- X$
125 GeV/c
M=4.0-8.5 GeV
y≥0
K=2.25± 0.45
$\langle K_T^2 \rangle = 0.88$ (GeV/c)^2
ANNIHILATION
INTRINSIC
COMPTON
$d\sigma/P_T dP_T$ cm^2 (GeV/c)$^{-2}$/nucleon
P_T (GeV/c)

Fig. 7

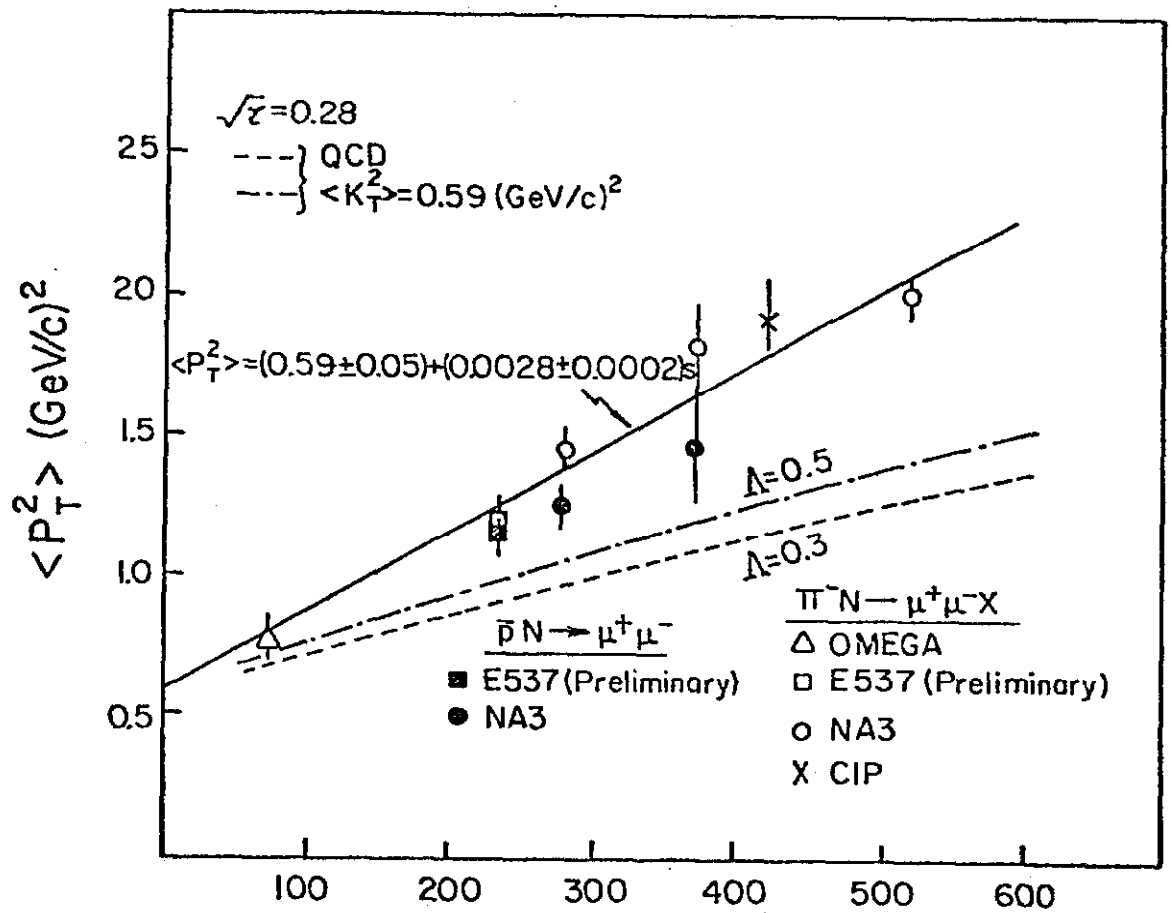
√τ=0.28
QCD
<K_T^2>=0.59 (GeV/c)^2
<P_T^2>=(0.59±0.05)+(0.0028±0.0002)S
Λ=0.5
Λ=0.3
p̄N→μ⁺μ⁻
E537 (Preliminary)
NA3
π⁻N→μ⁺μ⁻X
OMEGA
E537 (Preliminary)
NA3
CIP
<P_T^2> (GeV/c)^2
S (GeV^2)

Fig. 8a

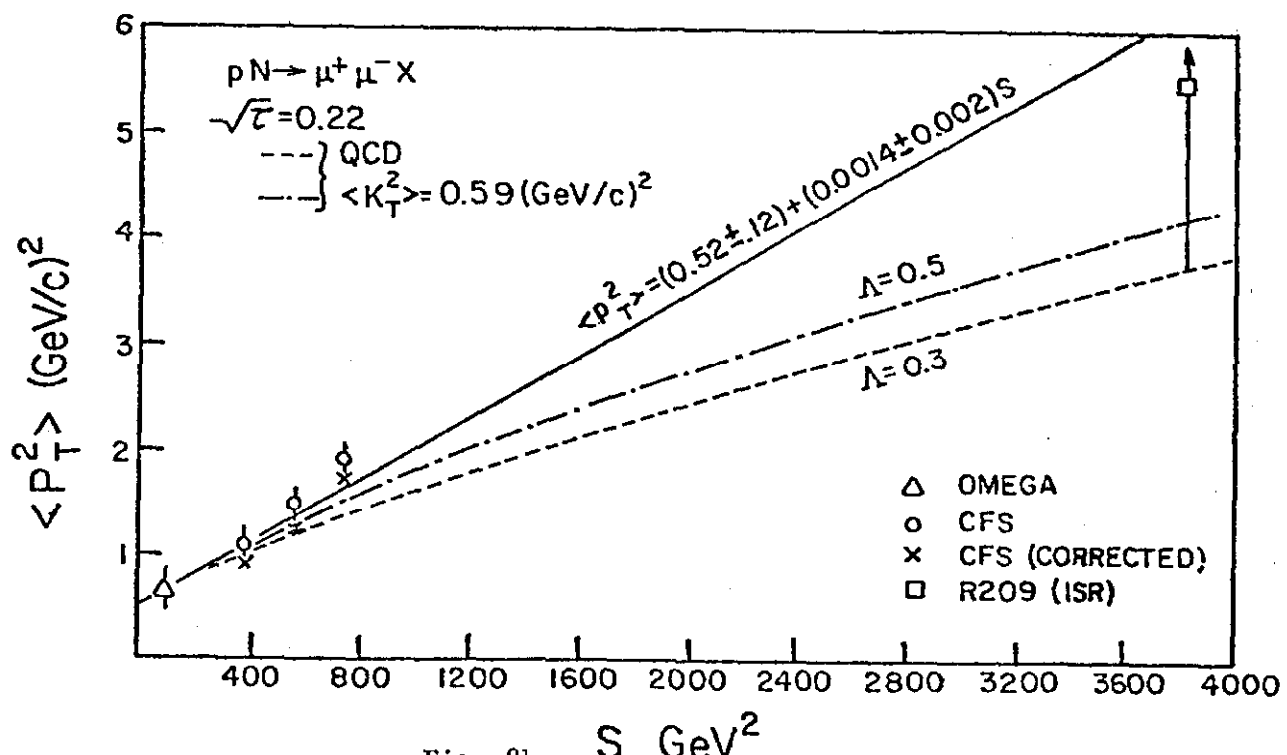
pN→μ⁺μ⁻X
√τ=0.22
QCD
<K_T^2>=0.59 (GeV/c)^2
<P_T^2>=(0.52±.12)+(0.0014±0.002)S
Λ=0.5
Λ=0.3
OMEGA
CFS
CFS (CORRECTED)
R209 (ISR)
<P_T^2> (GeV/c)^2
S GeV^2

Fig. 8b